Submitted to Atmospheric Science Letters, March 31, 2004; Revised, September 27, 2004; Accepted, October 6, 2004

# Ice and Water Permittivities for Millimeter and Sub-millimeter Remote Sensing Applications

**Jonathan H. Jiang and Dong L. Wu**

Jet Propulsion Laboratory, California Institute of Technology, Pasadena, California

**Abstract**

Recent advances in satellite remote sensing at near-millimeter and sub-millimeter wavelengths (~100-3000 GHz) require accurate complex permittivity for ice and liquid water at these frequencies for different temperatures, especially for cold atmospheric conditions. This paper summarizes the existing experimental permittivity data in the literature, and provides an updated empirical ice permittivity model for radiative transfer calculations for ground and space remote sensing experiments. Applications of this permittivity model to Microwave Limb Sounder (MLS) cloud measurements are discussed.

## 1. Introduction

Modeling cloud radiative properties requires accurate knowledge of the relative refractive index $m = m_1/m_o$ of ice and water hydrometers, where $m_1 = n' - in''$ is a complex refractive index and $m_o$ is the index of the surrounding medium. For the Earth's atmosphere, $m_0 = 1$, and $m$ is simply equal to the particle refractive index, which is the square root of the complex dielectric permittivity $\varepsilon$,

$$m = \sqrt{\varepsilon} \tag{1}$$

where

$$\varepsilon = \varepsilon' - i\varepsilon''. \tag{2}$$

The real part of the permittivity, $\varepsilon'$, the dielectric constant, is a parameter to describe how the electric field polarizes matter; the imaginary part, $\varepsilon''$, or loss factor, describes how electro-magnetic waves are absorbed.

The dielectric properties ($\varepsilon'$, $\varepsilon''$) of ice and water hydrometeors suspended in clouds play a key role in computing the radiative transfer under cloudy sky conditions, which can affect microwave propagation in the atmosphere. For the MLS cloud measurements, we developed an empirical model based on the parameterizations in *Liebe et al*. [1989, 1991] and *Hufford* [1991] (hereafter the LH model). The LH model was developed using empirical fits to published experimental data at frequencies < 1000 GHz for both ice and water, and limited to temperatures ≥ 0°C for water. The Earth Observing System (EOS) MLS instrument (which was launched onboard the EOS Aura Satellite on July 15, 2004) carries radiometers with frequencies up to 2500 GHz, most of which measure the atmosphere at very low temperatures (< 0°C). Therefore, permittivity models of ice and liquid water over a broader frequency interval are needed, especially for the imaginary part of the permittivity of ice at high frequencies (600-2500 GHz).

In this paper, we extend the original LH dielectric permittivity ($\varepsilon'$, $\varepsilon''$) model for pure ice to frequencies up to 3000 GHz and compare the updated parameterizations of ice and water permittivity to laboratory measurements reported in the literature. Applications of this extended model to Mie calculations and uncertainties at EOS MLS frequencies are discussed.

## 2. The complex permittivity for pure ice and water

For pure-water ice, the original LH model formulates the complex permittivity by

$$\begin{aligned} \varepsilon'_{ice} &= 3.15 \\ \varepsilon''_{ice} &= \alpha(T)/\nu + \beta(T)\nu \end{aligned} \tag{3}$$

where $\nu$ is frequency in GHz, and $\alpha(T)$ and $\beta(T)$ are temperature dependent parameters fitted to laboratory measurements [*Hufford* ,1991]. For pure liquid water, the formulations are:

$$\begin{aligned} \varepsilon'_{water} &= (\varepsilon_0 - 5.48)/[1+(\nu/\nu_P)^2] + 1.97/[1+(\nu/\nu_S)^2] + 3.51 \\ \varepsilon''_{water} &= (\varepsilon_0 - 5.48)(\nu/\nu_P)/[1+(\nu/\nu_P)^2] + 1.97(\nu/\nu_S)/[1+(\nu/\nu_S)^2] \end{aligned} \tag{4}$$

where $\varepsilon_0$ , $\nu_P$ and $\nu_S$ are all temperature dependent parameters [*Liebe et al.*, 1991].

To extend the LH formulae to frequencies >1000 GHz, we modified the LH expression for the imaginary part of the dielectric permittivity of ice by including a $\nu^3$ term in Equation (3), based on the far-infrared work by *Mishima et al*. [1983], namely

$$\varepsilon''_{ice} = \alpha(T)/\nu + \beta(T)\nu + \gamma\nu^3 , \tag{5}$$

where $\gamma$ can be calculated from the *B* factor in Equation (16) in *Mishima et al*. [1983] via the following. The additional *B* dependent absorption $K_a$ can be expressed as twice the attenuation coefficient $\alpha$ [*Ulaby, Moore and Fung*, 1981], i.e.,

$$K_a = 2\alpha = \frac{2\pi}{c} f \left|\mathrm{Im}\{\varepsilon\}\right| = \frac{2\pi}{c} f \frac{\varepsilon''}{\sqrt{\varepsilon'}} = B\left(\frac{f}{c}\right)^4 , \tag{6}$$

where $c$ is the speed of light in units of cm/s, $f$ is frequency in units of Hz, factor $B$ $=1.11\times10^{-6}\mathrm{cm}^{-4}$ is given by *Mishima et al*. [1983]. Rearranging Equation (6), we obtain an expression for the additional $\nu^3$ dependent permittivity $\varepsilon''$:

$$\varepsilon'' = \sqrt{\varepsilon'}\frac{B}{2\pi c^3} f^3 = 10^{27}\sqrt{\varepsilon'}\frac{B}{2\pi c^3}\nu^3 = \gamma\nu^3 . \tag{7}$$

The factor $10^{27}$ is the result of changing the frequency expression from $f$ (in Hz) to $\nu$ (in GHz). Substituting the values of $B$ and $c$, one obtains $\gamma = 10^{27}(\varepsilon')^{1/2} B/\left(2\pi c^3\right) = 1.16\times10^{-11}$.

For the real part of the ice permittivity, we assume the LH formula stays the same at higher frequencies, as do the real and imaginary parts of the permittivity of water.

## 3. Comparisons to laboratory measurements

### 3.1 The permittivity of pure ice

Laboratory measurements of the imaginary part of the ice refractive index or dielectric permittivity have been made and published by a number of researchers at millimeter and sub-millimeter wavelengths; they are summarized in Figure 1 with comparison to the modified LH model (Equation 5). The solid lines in Figure 1 show the imaginary ice dielectric permittivity computed by the modified LH model at different temperatures. The dotted lines are the original curves computed from the original LH formula (Equation 3). The measured data are described in the following.

*Mätzler and Wegmüller* [1987] presented measurements for the coefficient $\beta$ at temperatures between 0 and −30°C. The values of their $\varepsilon''$ at −3°C and −10°C in Figure 1 are estimated by using the modified LH formula. Note, however, *Mätzler and Wegmüller*'s $\beta$ is slightly different from the $\beta$ we used in Equation (3), specifically, their second term is $\nu^{1.2}$ for pure ice [*Matziler*, 1998]. *Perry and Straiton* [1973] obtained values of $\varepsilon'$ and $\varepsilon''$ from measurements at −28°C. *Mishima, Klug and Whalley* [1983] measured the absorption spectrum from 8-25 $cm^{-1}$ (400-1250 $\mu m$ wavelength or 240-750 GHz) for single crystals of ice at four temperatures (80, 100, 150, 202 *K*). The plotted values of the imaginary dielectric constant $\varepsilon''$ are estimated from their measurements of $n''$ at 202 *K* and assuming $\varepsilon'$ = 3.15. *Whalley and Labbe* [1969] measured the absorption spectrum from 17-42 $cm^{-1}$ (238-588 $\mu m$ wavelength or 510-1260 GHz) for blocks of ice at 100 and 200 *K*. We converted their measured values of $n''$ to $\varepsilon''$ also assuming $\varepsilon'$ = 3.15. *Berte, Labbe and Whalley* [1969] made measurements for thin films of ice (< 1 $\mu m$ thick) at 100 K from 100-8000 $cm^{-1}$ (or 3000GHz to 240 *THz*). The plotted $\varepsilon''$ are taken from their table III. They also presented some "preliminary and not very accurate" measurements of a 1-*mm* thick sample for 30-60 $cm^{-1}$ (900-1800 GHz) and estimated the value at 80 $cm^{-1}$ (2400 GHz).

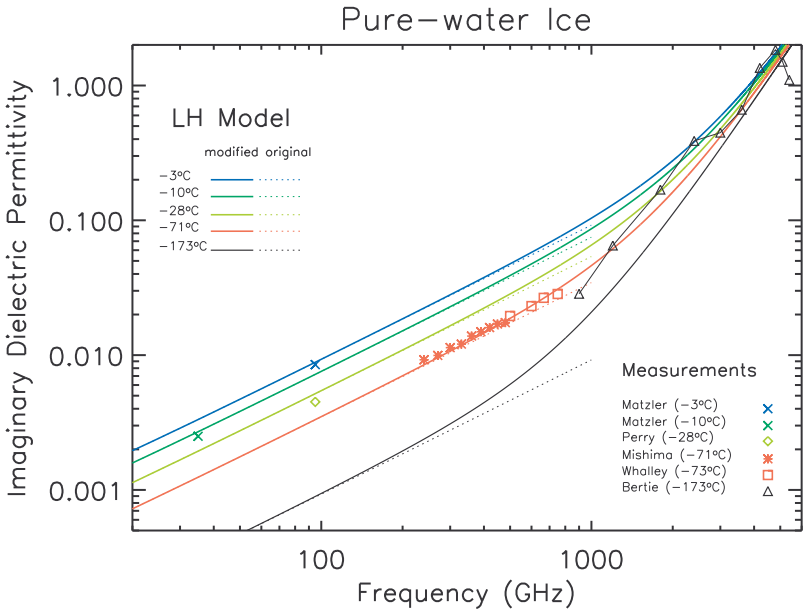


**Figure 1:** Computed and measured imaginary part of ice dielectric permittivity. The solid lines are ε″ computed using the modified LH formula (6), the dotted lines are those computed using the original LH formula (3).

In comparisons with the above laboratory data, we found the differences between the modified LH model results and the measurements is generally less than *~12%* for frequencies < 800 GHz and about *15-40%* at frequencies ≥ 3000 GHz. In the frequency range of 900-2400 GHz, the only available data are the preliminary measurements by *Berte, Labbe and Whalley* [1969], which may have large errors as stated in their paper. Also, we note that because of difficulties in accurately measuring $\varepsilon''$ of ice over the low frequency range (1-100 GHz) due to its low magnitude, large discrepancies still exist among other data sets derived from different experimental techniques. For example, *Koh*, [1997]'s results obtained using an interference technique at 75-110 GHz were a factor of ~3 lower than those of *Mätzler and Wegmüller*'s. Until additional experimental data become available, however, the modified LH model can be used to bridge the gaps between various data sets.

The measured values for the real part of ice permittivity $\varepsilon'$ are shown on Figure 2. The data labeled 'from Ulaby' are taken from *Ulaby, Moore and Fung* [1981], which consisted of a set of measurements by *Cumming* [1952], *Hippel* [1954], *Vant et al*. [1974], *Lamb* [1946], *Lamb and Turney* 1949, *Perry and Straiton* 1973. Other data are from *Bertie et al*. 1969.

The measurements of real permittivity of ice remain fairly constant over the broad microwave spectrum. Differences between the various measured data and the LH model value of 3.15 (shown as the straight line in Figure 2) are generally less than *5%* at frequencies < 1000 GHz. At higher frequencies (> 1000 GHz) the differences increase slightly but remain *<15%* in general.

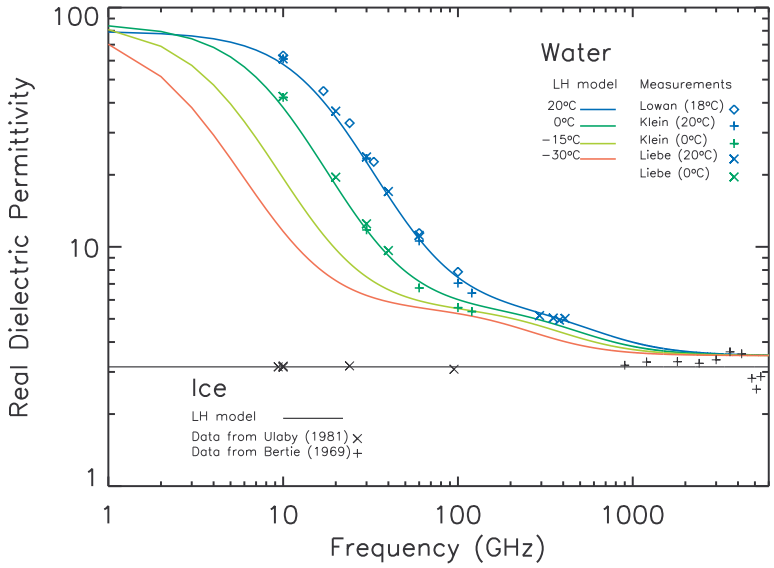


**Figure 2:** Computed and measured real part of ice and water dielectric permittivity. The solid curves are ε′ computed using the modified LH formula (3) for ice and (4) for liquid water.

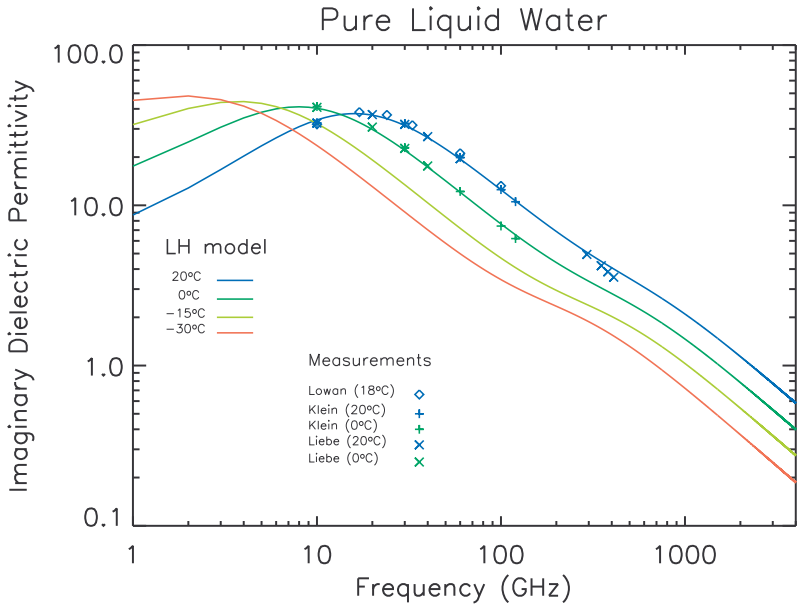


**Figure 3:** Computed and measured imaginary part of liquid water dielectric permittivities. The solid curves are ε′ computed using the modified LH formula (4).

3.2 The permittivity for pure liquid water

For liquid water, the measured real and imaginary parts of dielectric permittivity are shown in Figure 2 and Figure 3, respectively. Measurements by *Lowan* [1949], *Klein and Swift* [1977] were at frequencies mainly below 120 GHz, while the data from *Liebe et al.* [1991] are in the range from 5-410 GHz for temperatures ≤ 20°C.

The differences between measurements and the LH model are generally less than *~5%*. However, few measurements are made below 0°C. Values of the dielectric permittivity of super-cooled pure liquid water (< 0°C) are mostly computed from models [e.g. *Ulaby et al.* 1981, (p2020-2025); *Hulst* 1981, (p281-284)].

## 4. Sensitivity in microwave remote sensing applications

Cloud measurements using passive microwave instruments from space are relatively new and have important atmospheric applications. For example, recent observations with the limb-viewing MLS instrument onboard the Upper Atmosphere Research Satellite (UARS) on cloud occurrence frequency and cloud ice content in the upper troposphere have important applications in research related to the convective scale perturbations in the tropical tropopause layer (TTL) and their potential influence on stratospheric dehydration [e.g. *Jiang et al.*, 2004, *Read et al*., 2004; *Wu et al*. 2004].

Ice particles and water droplets have different Mie radiative properties in cold air conditions, mainly caused by their permittivity differences. Figure 4a shows the Mie extinction (solid lines) and scattering (dotted lines) efficiencies calculated at four selected MLS frequencies for ice particles (blue) and water droplets (red) at diameters between 1-4000 microns. The complex permittivities for ice and liquid water are computed for typical mid- to upper-tropospheric temperatures of –60°C and –15°C, respectively. From this example we see that the Mie extinction and scattering efficiencies of small liquid water particles (diameter < 500 $\mu m$) are much higher than those of small ice particles. Most importantly, for these ice particles, which account for most cloud ice content in the upper-troposphere, scattering occurs nearly in the Rayleigh regime at the MLS frequencies. In other words, for most upper-tropospheric clouds, the Mie coefficient increases with ice particle size.

The Mie phase function depends mainly on the particle size parameter ($\chi = 2\pi r/\lambda$), but it is also influenced by the complex permittivity. Figure 4b illustrates the computed phase functions for single ice particles and water droplets with various particle size parameters. The dielectric permittivity values are computed for ice or water at 203 GHz using the same temperatures as in Figure 4a. The single scattering albedo ($\omega_0$) shown for each particle size is the ratio of Mie scattering to extinction efficiencies. For small size parameter (e.g. $\chi < 0.1$), both ice and water scatter radiation in nearly equal quantities forwards and backwards and the single scattering albedo is small. For large size parameter (e.g. $\chi > 1$), the radiation is heavily concentrated in a narrow forward lobe, the single scattering albedo increases, and the ice and water phase functions become different. At very large size parameter (e.g. $\chi = 10$), the backward scattering of ice particles is much larger than that of liquid droplets. Also notably, the single scattering albedo of ice ($\omega_{0\_i}$) is much larger than that of water ($\omega_{0\_w}$) for all particle sizes, mainly due to the difference in Mie efficiencies.

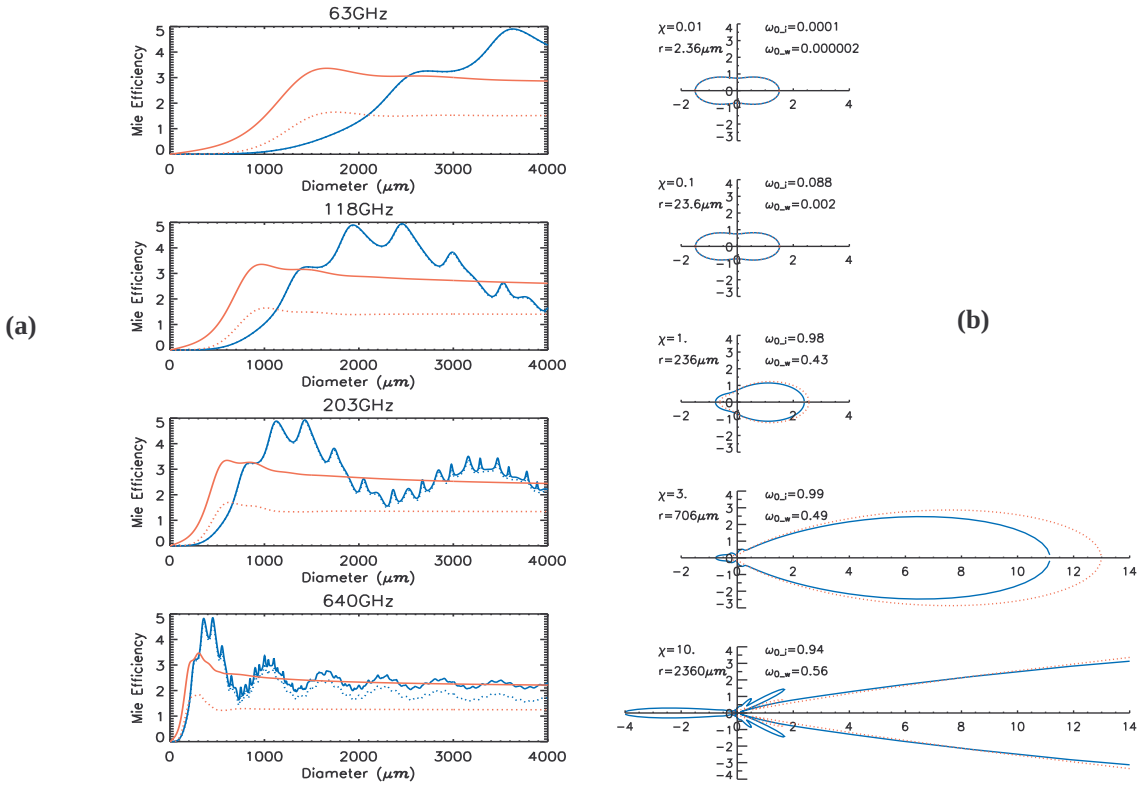


**Figure 4:** (a) Mie extinction (solid line) and scattering (dotted line) efficiencies for ice (blue) and liquid water (red); (b) Phase function for single ice particles (solid line) and water droplet (dotted line) with different size parameters. The complex dielectric permittivities are computed at −60°C for ice and −15°C for liquid water.

| **Typical MLS Radiometers** | **T** (°C) | **ε′** | **ε″** | **$\xi_e$** | **$\lvert\Delta\xi_e\rvert$** (Δε′=5%) | **$\lvert\Delta\xi_e/\xi_e\rvert$** (Δε′=5%) | **$\lvert\Delta\xi_e\rvert$** (Δε″=20%) | **$\lvert\Delta\xi_e/\xi_e\rvert$** (Δε″=20%) | **$\omega_0$** | **$\lvert\Delta\omega_0\rvert$** (Δε′=5%) | **$\lvert\Delta\omega_0\rvert/\omega_0$** (Δε′=5%) | **$\lvert\Delta\omega_0\rvert$** (Δε″=20%) | **$\lvert\Delta\omega_0/\omega_0\rvert$** (Δε″=20%) |
|---|---|---|---|---|---|---|---|---|---|---|---|---|---|
| 63 GHz | −15 | 3.15 | 0.0042 | 0.000397 | .0000027 | **0.7%** | .00005 | **12.9%** | 0.356 | 0.033 | **9.3%** | 0.041 | **11.4%** |
| | −30 | | 0.0033 | 0.000342 | .0000005 | **0.1%** | .00004 | **11.7%** | 0.414 | 0.035 | **8.4%** | 0.043 | **10.5%** |
| | −60 | | 0.0024 | 0.000287 | .0000036 | **1.3%** | .00003 | **10.1%** | 0.493 | 0.035 | **7.1%** | 0.045 | **9.2%** |
| 118 GHz | −15 | 3.15 | 0.0079 | 0.00269 | 0.00010 | **3.7%** | 0.0002 | **6.9%** | 0.654 | 0.031 | **4.7%** | 0.042 | **6.5%** |
| | −30 | | 0.0062 | 0.00249 | 0.00011 | **4.5%** | 0.0001 | **5.9%** | 0.707 | 0.028 | **4.0%** | 0.039 | **5.5%** |
| | −60 | | 0.0045 | 0.00229 | 0.00012 | **5.3%** | 0.0001 | **4.6%** | 0.768 | 0.024 | **3.1%** | 0.034 | **4.4%** |
| 190 GHz | −15 | 3.15 | 0.0128 | 0.0147 | 0.00095 | **6.4%** | 0.0005 | **3.5%** | 0.822 | 0.019 | **2.4%** | 0.028 | **3.4%** |
| | −30 | | 0.0100 | 0.0142 | 0.00096 | **6.9%** | 0.0004 | **2.9%** | 0.855 | 0.016 | **1.9%** | 0.024 | **2.8%** |
| | −60 | | 0.0073 | 0.0136 | 0.00100 | **7.4%** | 0.0003 | **2.2%** | 0.890 | 0.013 | **1.4%** | 0.019 | **2.2%** |
| 203 GHz | −15 | 3.15 | 0.0137 | 0.0189 | 0.00127 | **6.7%** | 0.0006 | **3.4%** | 0.839 | 0.018 | **2.1%** | 0.026 | **3.1%** |
| | −30 | | 0.0107 | 0.0183 | 0.00131 | **7.2%** | 0.0005 | **2.6%** | 0.869 | 0.015 | **1.7%** | 0.022 | **2.5%** |
| | −60 | | 0.0078 | 0.0176 | 0.00134 | **7.6%** | 0.0003 | **2.0%** | 0.901 | 0.012 | **1.3%** | 0.017 | **1.9%** |
| 240 GHz | −15 | 3.15 | 0.0162 | 0.0359 | 0.00268 | **7.5%** | 0.0009 | **2.5%** | 0.875 | 0.014 | **1.6%** | 0.021 | **2.4%** |
| | −30 | | 0.0127 | 0.0350 | 0.00273 | **7.8%** | 0.0007 | **2.0%** | 0.899 | 0.011 | **1.3%** | 0.018 | **2.0%** |
| | −60 | | 0.0093 | 0.0340 | 0.00277 | **8.1%** | 0.0005 | **1.5%** | 0.924 | 0.009 | **1.0%** | 0.014 | **1.5%** |
| 640 GHz | −15 | 3.15 | 0.0458 | 1.413 | 0.19014 | **13.5%** | 0.0101 | **0.7%** | 0.945 | 0.004 | **0.4%** | 0.010 | **1.1%** |
| | −30 | | 0.0366 | 1.403 | 0.19027 | **13.6%** | 0.0081 | **0.6%** | 0.956 | 0.003 | **0.4%** | 0.008 | **0.9%** |
| | −60 | | 0.0274 | 1.392 | 0.19039 | **13.7%** | 0.0061 | **0.4%** | 0.967 | 0.002 | **0.2%** | 0.006 | **0.7%** |
| 2500 GHz | −15 | 3.15 | 0.4906 | 2.380 | 0.07139 | **3.0%** | 0.0439 | **1.8%** | 0.470 | 0.021 | **4.4%** | 0.012 | **2.6%** |
| | −30 | | 0.4544 | 2.353 | 0.08254 | **3.5%** | 0.0448 | **1.9%** | 0.481 | 0.022 | **4.8%** | 0.016 | **3.3%** |
| | −60 | | 0.4187 | 2.323 | 0.09618 | **4.1%** | 0.0452 | **1.9%** | 0.495 | 0.025 | **5.0%** | 0.020 | **4.0%** |

**Table 1:** For each typical UARS and EOS MLS radiometer frequency, this table lists the Mie extinction coefficient ($\xi_e$), single scattering albedo ($\omega_0$) for a typical ice particle of 200 μm diameter at three different temperatures (−15°C, −30°C and −60°C), and their percentage errors resulting from a 20% uncertainty in the imaginary part of ice permittivity (blue) or a 5% uncertainty in the real part of ice permittivity (green).

In practice, we have found ice particles with diameters of ~100-300 $\mu m$ produce the strongest signatures in UARS MLS radiances [*Wu et al*. 2004]. Scattering by such particles occurs in the Rayleigh regime for MLS frequencies ≤ 640 GHz. From our calculations summarized in Table 1, a *20%* uncertainty in the imaginary part of permittivity for an ice particle in that size range will result in *~1%* to *10%* errors in both the Mie extinction coefficients and the single scattering albedos at typical MLS measurement frequencies. For 640 GHz, the error is about *1%* or less, which could be the best for the cloud measurement in the TTL [*Wu and Jiang*, 2004]. Similar uncertainties in the real part of permittivity will result in larger errors, e.g. a *5%* uncertainty will result *~1% to 10%* error in typical MLS frequencies. Fortunately, the measured value for the real part of ice permittivity is more certain at the MLS frequency range.

## 5. Summary

The empirical model of dielectric ice permittivity is extended to frequencies as high as 3000 GHz from the original LH formulae. The modified LH model may have uncertainties of about *12%* in the imaginary part and of *5%* in the real part of ice permittivity at a frequency range of 100-1000 GHz in comparisons with laboratory data. At higher frequencies (>1000GHz) the uncertainties may be up to *~50%* in the imaginary part and *~15%* in the real part, respectively. For liquid water, uncertainties are *5%* or less in both imaginary and real parts of the permittivity for temperature ≤ 0°C. Additional uncertainties may exist at lower temperatures where little laboratory measurements are available.

Such uncertainties in ice and water permittivity may result in about *10-20%* in combined errors in the Mie theory calculations. Thus more laboratory measurements are needed to improve our knowledge of permittivity. Also, our empirical model is based only on pure ice and liquid water. Impurity effects on ice permittivity are little known, such as those formed in polar stratospheric clouds (PSCs). Although this study is primarily motivated by the current MLS cloud studies, it also has important applications to other ground, airborne, and space microwave sensors.

## Acknowledgements

The authors wish to express their gratitude to Christian Mätzler, Joe Waters, Paul Wagner and Van Snyder for helpful comments and suggestions. This work was conducted at the Jet Propulsion Laboratory, California Institute of Technology, under contract with the National Aeronautics and Space Administration.

## References

Cumming, W.A., The dielectric properties of ice and snow at 3.2 centimeters, *J. Appl. Phys*., 23, 768-773, 1952.

Bertie, J.E., H.J. Labbe, and E. Whalley, Absorptivity of ice I in the range 4000-30 $cm^{-1}$, *J. Chem. Phys*., 50, 4501-4520, 1969.

Hufford, G., A model for the complex permittivity of ice at frequencies below 1 THz. *Int. J. Infrared Millimeter Waves*, 12, 677-682, 1991.

von Hippel, A. (ed), *Dielectric Materials and Applications*, MIT Press, Cambridge, MA, 1945.

von de Hulst, H. C., *Light Scattering by Small Particles*. pp 470, New York, Dover, 1981.

Jiang, J.H, B. Wang, K. Goya, K. Hocke, S.D. Eckerman, J. Ma, D.L. Wu, W.G. Read, Geographical distribution and inter-seasonal variability of tropical deep convection: UARS MLS observations and analyses," *J. Geophys. Res*. 109, D3, D03111, 10.1029/2003JD003756,2004.

Klein, L.A., and C.T. Swift, An improved model for the dielectric constant of sea water at microwave frequencies, *IEEE Transactions on Antennas and Propagation*, Vol. 25, 1977.

Koh, G., Dielectric properties of ice at millimeter wavelengths, *Geophys., Res. lett*., Vol. 24, 2311-2313.
Lamb, J., Measurements of the dielectric properties of ice, *Discuss. Faraday Soc*., 42A, p238, 1946.
Lamb, J., and A. Turney, The dielectric properties of ice at 1.25 cm. wavelength, *Proc. Phys. Soc*. London Sect., B 62, 272-273, 1949.
Liebe, H. J., T. Manabe, and G. A. Hufford, Millimeter-wave attenuation and delay rates due to fog/cloud conditions. IEEE Trans. *Ant. Prop*., **37**, 1617-1623, 1989.
Liebe, H. J., G. A. Hufford, and T. Manabe, A model for the complex permittivity of water at frequencies below 1 THz, *Int. J. Infrared and Millimeter Waves*, 12-7, 659-674, 1991.
Lowan, A.N., Tables of Scattering functions for spherical particles, U.S. National Bureau of Standards, *Applied Mathematics Series* 4, 1949.
Matzler, C., Microwave properties of ice and snow, *Solar System Ices*, B. Schmitt et al. (eds.), 241-257, Kluwer Academic Publishers, 1998.
Matzler, C., and U. Wegmuller, Dielectric properties of freshwater ice at microwave frequencies, *J. Phys. D: Appl. Phys*., 20, 1623-1630, 1987.
Mishima, O., D. D. Klug, and E. Wahlley, The far-infrared spectrum of ice Ih in the range 8-25cm$^{-1}$. Sound waves and difference bands, with application to Saturn's rings. *J. Chem .Phys*., 78, 6399-6404, 1983.
Perry, J., and A.W. Straiton, Revision of dielectric-constant of ice in millimeter-wave spectrum, *J. Appl. Phys*., 44(11), 5180-5180, 1973.
Read, W.G., D.L. Wu, J.W. Waters, H.C. Pumphrey, Dehydration in the tropical tropopause layer: Implications from UARS MLS," *J. Geophy. Res*., 109, D6, D06110, 10.1029/2003JD004056, 2004.
Whalley, E., and H.J. Labbe, Optical Spectra of Orientationally Disordered Crystals. III. Infrared Spectra of the Sound Waves, *J. Chem. Phys.*, **51**, 3120-3127, 1969.
Ulaby, F. T., Moore, R. K., and Fung, A. K., *Microwave Remote Sensing: Active and Passive, Volume I: Microwave Remote Sensing Fundamentals and Radiometry*, Artech House, Inc., 1981.
Vant, M.R., R.B. Gray, R.O. Ramseier, and V. Makios, Dielectric properties of fresh and sea ice at 10 and 35 GHz, *J. Appl. Phys*., 45, p4712, 1974.
Wu, D.L., W.G. Read, A.E. Dessler, S.C. Sherwood, J.H. Jiang, UARS MLS cloud ice measurements and implications for H2O transport near the tropopause, *J. Atmos. Sci*., in press, 2004.
Wu, D. L., and J. H. Jiang, EOS MLS Algorithm Theoretical Basis for Cloud Measurements, *Technical Report*, Jet Propulsion Laboratory, *D-19299/CL#04-2160, EOS MLS DRL 601(part 6), ATBD-MLS-06*, 2004. (For additional information visit http://mls.jpl.nasa.gov/jonathan/cloud_ice/)